Progress In Electromagnetics Research, Vol. 138, 479–497, 2013

STATISTICAL CHARACTERISTICS OF THE MULTI-PATH TIME DELAY AND DOPPLER SHIFT OF A RADAR WAVE PROPAGATING THROUGH THE IONOSPHERE

Bao-Ke Ma[1, 2, *], Li-Xin Guo[1], and Hong-Tao Su[1]

[1]School of Science, Xidian University, No. 2 Taibai Road, Xi'an, Shaanxi, China

[2]School of Science, Xi'an Polytechnic University, No. 19 JinHua Road, Xi'an, Shaanxi, China

Abstract—Multi-path time delay spread is a very important factor in the bit error rate of high-frequency ionospheric communication channels and in the target detection performance of over-the-horizon radars. In this study, the probability density distribution of multi-path time delay and Doppler shift of ionospheric radio signal are derived using Rayleigh fading. Moreover, the probability density distribution of time delay, average power of the received signal, and received signal variance are discussed in detail. Using a designed experimental circuit, the measured value of the multi-path time delay spread is obtained from three given radio paths by the sweep-frequency pulse sounding technique. The average value of the multi-path time delay spread that changes with the ratio K, which is the operating frequency of the basic maximum usable frequency, is also analyzed and fitted using the least-squares fitting method. Theoretical and statistical research shows that for a given radio path and specific frequency, the multi-path time delay spread approximately follows a normal distribution. The average time delay spread decreases with the increase in the ratio K; however, it eventually approaches a steady value. The results of this research provide an empirical reference for further prediction and estimation of the time delay spread of a radar wave propagating through the ionosphere.

Received 25 January 2013, Accepted 22 March 2013, Scheduled 1 April 2013

* Corresponding author: Bao-Ke Ma (Baokema2006@126.com).

1. INTRODUCTION

The characteristics of the high-frequency (HF) ionospheric channel are time varying. Based on its influence on radio wave propagation, it can be described as a linear time-varying channel. In physics, the received signal can be viewed as a multi-path signals superposition with different time delays, frequency shifts and incident angles (Figure 1) [1, 2]. As early as 1980s, Maresca and Georges indicated that the spectrum quality of the sea surface echo for the over-the-horizon radar is closely related to the changes in the ionosphere [3]. Given the random time-varying characteristic of the ionospheric medium, the multi-path time delay and Doppler shift effects are the main features for the HF radar wave propagating through the ionosphere [2].

For multi-path time delay estimation, the classic match filtering technique was proposed by Bell and Ewart [4]. However, the estimation accuracy of this method is based on the main peak width of the autocorrelation function of the transmitted signals. Thus, high-resolution frequency domain estimation methods, such as MUSIC, ESPRIT, and the linear prediction, have been proposed by some scholars to estimate the time delay. However, a satisfactory estimation of the multi-path time delay is obtained only for signals with flat or almost flat spectra [5, 6]. In addition, the maximum likelihood estimation and the least-squares algorithm are used to estimate the time delay [7], but their processes involve more complex multidimensional optimization. For an adaptive system, the methods of multi-path cancelation and multi-path equalization were used by Ching and So to estimate time delay [8]. A new method for estimating the Doppler shift and time delay of the overlapping echoes was presented by Qi et al. [9] and Zhang et al. [10]. Other methods, such as the statistical moment method, have been used by some scholars to estimate the multi-path time delay and Doppler shift spread [11, 12].

For the echo field of a radio wave, a model of a random moving rough scattering screen was used by Booker et al., Essex et al., and Baussard et al. to analyze the autocorrelation coefficient of the amplitude and field strength distribution [13–15], and some analytical formulas for Doppler shift and bandwidth of radar echoes backscattered from time-varying sea surface are derived by Wang et al. and Nie et al. [16, 17]. Moreover, From and Meehan studied the characteristics of the HF Doppler echo and its change rule caused by the ionospheric irregularities [18]. Cornelius and Essex used the HF Doppler technology to observe the changes in the Doppler spectrum caused by the movement of the Sporadic E and the expansion of the F region of the ionosphere [19]. A more concise relationship

between the Doppler shift and radio wave frequency was presented by Long and Hou [20], Ma et al. [21], Davies and Baker [22], Lee et al. [23]. Based on the ray theory [24] and consideration the time-varying anisotropic lossless ionosphere, a more general expression for the Doppler frequency shift was provided by Bennett [25]. In the present research, the probability density distribution of the multi-path time delay and Doppler shift are derived using random signal processing techniques [26] with Rayleigh fading. The probability density distributions of the multi-path time delay, average power of the received signal, and signal variance changes with the time delay spread are discussed in detail. Based on the designed experiment circuit and using the sweep-frequency pulse sounding technique, the average value of the multi-path time delay spread changes with the ratio K is also analyzed and fitted using the LS algorithm. Compared with the methods mentioned early, the proposed method in this paper is more concise, simpler, and has a clear physical meaning.

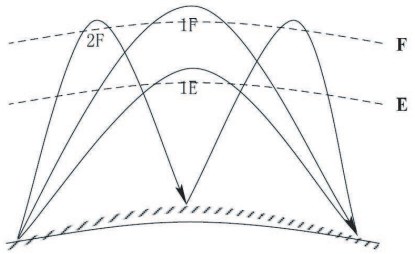

Figure 1. Diagram of the multi-path and multi-mode propagation of the sky wave through the ionosphere.

2. THEORETICAL ANALYSIS

2.1. Joint Probability Density Function (PDF) for the Instantaneous Power and q Variable

Statistical analysis shows that the amplitude fading of HF ionospheric signal follows the Rayleigh distribution. With Rayleigh fading, the field of the received signal can be expressed as [27–30]

$$E = E_0 e^{j\Phi} = X + jY = \sum_k a_k e^{j\theta_k} \tag{1}$$

where $E_0^2 = X^2 + Y^2$, $\Phi = \arctan\frac{Y}{X}$, $X = \sum_k a_k \cos\theta_k$, and $Y = \sum_k a_k \sin\theta_k$ follow the normal distribution with zero mean and the same

variance. E_0 and a_k meet the Rayleigh distribution. θ_k and Φ satisfy the uniform distribution.

If we let variable ξ represent time t or angular frequency ω, the following relationship can be obtained with Equation (1):

$$\frac{d\Phi}{d\xi} = \frac{1}{E_0^2}\left(X\frac{dY}{d\xi} - Y\frac{dX}{d\xi}\right) \tag{2}$$

Furthermore, if we let $q = d\Phi/d\xi$, $U = dY/d\xi$ and $V = -dX/d\xi$, Equation (2) can be simplified as

$$q = \frac{d\Phi}{d\xi} = \frac{1}{E_0^2}(XU + YV) \tag{3}$$

In Equation (3), when ξ represents the dimension of time τ, variable q corresponds to the angular frequency ω, thereby reflecting the instantaneous Doppler shift of the received signal. On the contrary, when ξ represents the angular frequency ω, the variable q corresponds to the time τ, thereby reflecting the instantaneous multi-path time delay or group delay of the received signal.

We define variable δ as the relative ratio of the amplitude of the received signal to the variable ξ as follows:

$$\delta = \frac{1}{E_0}\frac{dE_0}{d\xi} = \frac{YU - XV}{E_0^2} \tag{4}$$

All these features indicate that if variables X and Y follow a normal distribution, the result V (or U) of variable X (or Y) derivative with respect to time τ or frequency ω also meets the normal distribution. Thus, the joint PDF of X, Y, U and V can be expressed as [20]

$$\begin{aligned} P(X,Y,U,V) &= \frac{1}{(2\pi)^{d/2}|B|^{1/2}}\exp\left(-\frac{1}{2}(\mu_1,\mu_2,\mu_3,\mu_4)^T B^{-1}(\mu_1,\mu_2,\mu_3,\mu_4)\right) \\ &= \frac{1}{(2\pi)^2\sqrt{M}}\exp\left(-\frac{1}{2M}\sum_{i,j=1}^{4} M_{i,j}\mu_i\mu_j\right) \end{aligned} \tag{5}$$

In Equation (5), B denotes the covariance matrix, M the value of the determinant B, $M_{i,j}$ the algebraic complement of the element $b_{i,j}$ of the matrix B, and $b_{i,j} = \overline{\mu_j\mu_i}$ $(i, j = 1, 2, 3, 4)$, where $\mu_1 = X$, $\mu_2 = Y$, $\mu_3 = V - \bar{V}$, and $\mu_4 = U - \bar{U}$.

Assuming that $\sigma(\eta)$ is the spectral function of the transfer function that corresponds to the autocorrelation function $S(\xi)$ on the ξ axis, the average multi-path time delay or average Doppler frequency shift spread (i.e., the normalized average value of the spectrum of the time

delay or of the frequency shift) can be defined as

$$\bar{q} = \frac{\int \eta\sigma(\eta)d\eta}{\int \sigma(\eta)\,d\eta} \tag{6}$$

The average envelope power of the transmitting signal can be defined as

$$\alpha^2 = \int \sigma(\eta)\,d\eta \tag{7}$$

The signal variance is defined as

$$\beta^2 = \int \eta^2\sigma(\eta)\,d\eta - \left(\int \eta\sigma(\eta)d\eta\right)^2 \tag{8}$$

Combined with Equations (5) to (8), the joint PDF of Equation (5) can be further expressed as

$$\begin{aligned} P(X,Y,U,V) \;=\; & \frac{1}{(\pi\alpha\beta)^2}\exp\left[-\frac{1}{\beta^2}\left(\frac{\beta^2}{\alpha^2}+\bar{q}\right)^2\left(X^2+Y^2\right)\right. \\ & \left.-\left(U^2+V^2\right)\frac{1}{\beta^2}+\frac{2\bar{q}}{\beta^2}(XU+YV)\right] \end{aligned} \tag{9}$$

Based on Equations (1) to (4) and the joint PDF of X, Y, U and V, the joint PDF of variable E_0^2, Φ, q and δ can be expressed as

$$P\left(E_0^2,\delta,\Phi,q\right) = \frac{E_0^2}{2\pi^2\alpha^2\beta^2}\exp\left[-\frac{E_0^2}{\alpha^2}-\frac{E_0^2\delta^2}{\beta^2}-\frac{E_0^2}{\beta^2}(q-\bar{q})^2\right] \tag{10}$$

Using the boundary integral method for variables δ and Φ in Equation (10), the joint PDF for E_0^2 and q can be written as

$$P\left(E_0^2,q\right) = \frac{E_0}{\sqrt{\pi}\alpha^2\beta}\exp\left(-\frac{E_0^2}{\alpha^2}\right)\exp\left[-\frac{E_0^2(q-\bar{q})}{\beta^2}\right] \tag{11}$$

Equation (11) shows that the joint PDF for signal strength and multi-path time delay have the same mathematical expressions as the signal strength and the Doppler shift. The only difference is the values of parameters α, β, and $\bar{q}$, as well as their physical meaning.

2.2. PDF of the Multi-path Time Delay and the Doppler Shift

Using the boundary integral method for variable E_0^2 in Equation (11), the PDF for q can be written as

$$P(q) = \frac{\alpha}{2\beta}\left[1+\frac{\alpha^2}{\beta^2}(q-\bar{q})^2\right]^{-3/2} \tag{12}$$

Thus, the PDF function for multi-path time delay and Doppler shift can be expressed as

$$P(\tau) = \frac{1}{M}\left[1 + \frac{4}{M^2}(\tau - \bar{\tau})^2\right]^{-3/2} \quad \text{multi-path time delay} \tag{13}$$

$$P(f) = \frac{1}{D}\left[1 + \frac{4}{D^2}\left(f - \bar{f}\right)^2\right]^{-3/2} \quad \text{Doppler shift} \tag{14}$$

where $M = 2\beta/\alpha$ denotes the multi-path time delay spread, and $\bar{\tau}$ is the normalized average value of the delay power spectrum $\sigma(\tau)$. Compared with Equation (13), $D = 2\beta/\alpha$ represents the Doppler shift spread, and $\bar{f}$ represents the normalized average value of the frequency shift power spectrum $\sigma(f)$. Equations (13) and (14) show that the PDF of the multi-path time delay (or Doppler shift) is closely related to the first- and second-order moment of the time delay power spectrum (or the frequency shift power spectrum) only. In other words, although the specific forms of the delay power spectrum and the frequency shift power spectrum are different, they have the same first- and second-order moments. Therefore, the value of the probability density of the multi-path time delay or Doppler frequency shift should is the same.

2.3. Average Power of the Received Signal

Based on Equation (11) and variable q, the average received power of the radio wave can be defined as

$$\bar{I}(q) = \frac{\int_0^\infty IP\left(E_0^2, q\right) dI}{\int_0^\infty P(I, q)\, dI} = \frac{3\alpha^2}{2}\left[1 + \frac{\alpha^2 (q - \bar{q})^2}{\beta^2}\right]^{-1} \tag{15}$$

The average power of the received signal for the multi-path time delay and Doppler frequency shift can be expressed as

$$\bar{I}(\tau) = \frac{3\alpha^2}{2}\left[1 + \frac{4(\tau - \bar{\tau})^2}{M^2}\right]^{-1} \tag{16}$$

$$\bar{I}(f) = \frac{3\alpha^2}{2}\left[1 + \frac{4\left(f - \bar{f}\right)^2}{D^2}\right]^{-1} \tag{17}$$

As shown in Equations (16) and (17), the average power of the received signal achieves the maximum value at the average value of the delay power spectrum $\bar{\tau}$ (or the frequency shift power spectrum $\bar{f}$). However, the average power of the received signal is reduced when the value of the multi-path time delay (or the Doppler shift) deviates from the average value of the power spectrum.

2.4. Signal Variance of the Multi-path Time Delay and Doppler Shift

Using the instantaneous power I as a variable, the variance of the variable q can be expressed as

$$\sigma_q^2(I) = \frac{\int_{-\infty}^{\infty} q^2 P(I,q)\,dq}{\int_{-\infty}^{\infty} P(I,q)\,dq} - \left[\frac{\int_{-\infty}^{\infty} qP(I,q)\,dq}{\int_{-\infty}^{\infty} P(I,q)\,dq}\right]^2 \tag{18}$$

Substituting Equation (11) into Equation (18), the following simplified formula is obtained

$$\sigma_q^2(I) = \beta^2/2I$$

The variance of the multi-path time delay and Doppler shift can be expressed as

$$\sigma_\tau^2(I) = \frac{M^2a^2}{8I} = M^2/8P_0 \quad \text{multi-path time delay} \tag{19}$$

$$\sigma_f^2\left(E_0^2\right) = \frac{D^2a^2}{8E_0^2} = D^2/8P_0 \quad \text{Doppler shift} \tag{20}$$

where $P_0 = I/\alpha^2$ denotes the normalized instantaneous power. The variance of the multi-path time delay σ_τ^2 (or the variance of the Doppler shift σ_f^2) is proportional to the square of the time delay spread M (or the Doppler shift spread D), and inversely proportional to the normalized instantaneous power P_0. If we know the first and second moments of the time delay spectrum or Doppler shift spectrum, the multi-path time delay, Doppler shift, instantaneous power, and other statistical parameters can be determined with Rayleigh fading and by using Equations (16)–(20).

3. NUMERICAL SIMULATION AND ANALYSIS

As shown by the theoretical analysis, the PDF, average power and variance of the received signal of the time delay have the same expression form as that of the Doppler shift. Thus, only the statistical characteristics of the multi-path time delay are simulated and analyzed.

3.1. Change in the Probability Density of the Multi-path Time Delay with Time Delay (Group Time Delay)

The change in the probability density of the multi-path time delay with the group time delay, and time delay spread M are shown in Figures 2

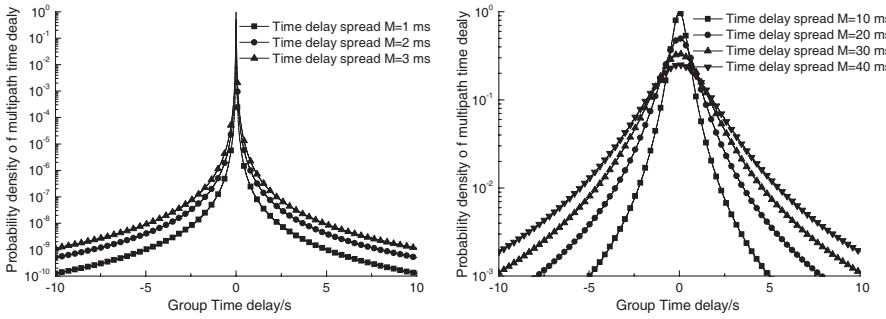

Figure 2. Change in the probability density of the multi-path time delay $P(\tau)$ with the time delay τ (group time delay), the normalized average value of the time delay spectrum $\bar{\tau} = 0\,\mathrm{s}$.

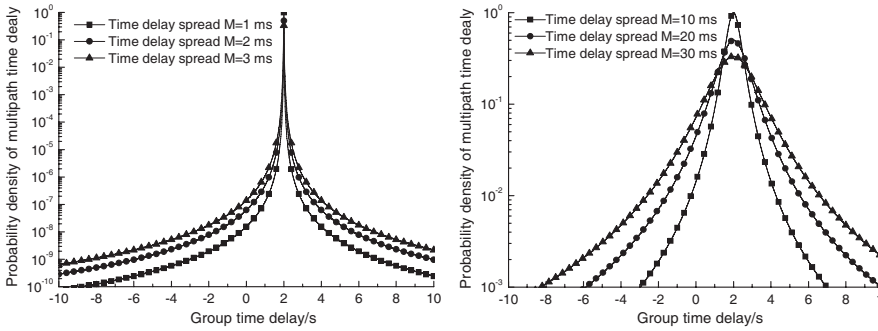

Figure 3. Change in the probability density distribution of the multi-path time delay $P(\tau)$ with the time delay τ (group time delay). The normalized average value of the time delay power spectrum $\bar{\tau} = 2\,\mathrm{s}$.

and 3. Figures 2(a), 2(b), 3(a), and 3(b) show that with Rayleigh fading, the probability density distribution of the multi-path time delay approximately meets the normal distribution and is symmetrically distributed about the normalized average value of the time delay spectrum $\bar{\tau}$. The probability density distribution function of the multi-path time delay can reach a maximum value at the normalized average value of the delay power spectrum $\bar{\tau}$. That is, the multi-path time delay is most likely to take the average value of the time delay spectrum. In addition, the greater the multi-path time delay deviation is from the average value of the time delay spectrum, the smaller the probability density is, which is easy to understand. Moreover, when the group time delay is close to the normalized average value of the time delay

spectrum $\bar{\tau}$, the probability density distribution of the multi-path time delay rapidly decreases with increased group time delay. When the group delay τ is much larger than the average value of the delay power spectrum $\bar{\tau}$, the probability density distribution of the multi-path time delay gradually changes.

3.2. Change in the Normalized Average Power of the Received Signal with Time Delay

As shown in Figures 4 and 5, when the transmitting signal power is given (here, $\alpha = 1\,\mathrm{J/s}$), the normalized average power of the received signal $\overline{I}$ approaches maximum value at the normalized average value of the time delay spectrum $\bar{\tau}$ as the probability density of the multi-path time delay changes. If the multi-path time delay deviates from the average value of the time delay spectrum $\bar{\tau}$, the normalized average power of the received signal considerably decreases. Moreover, the smaller the multi-path time delay spread M is, the faster the signal power decreases. In other words, the smaller the multi-path time delay spread M is in a given channel, the smaller the jitter range of the received signal power is.

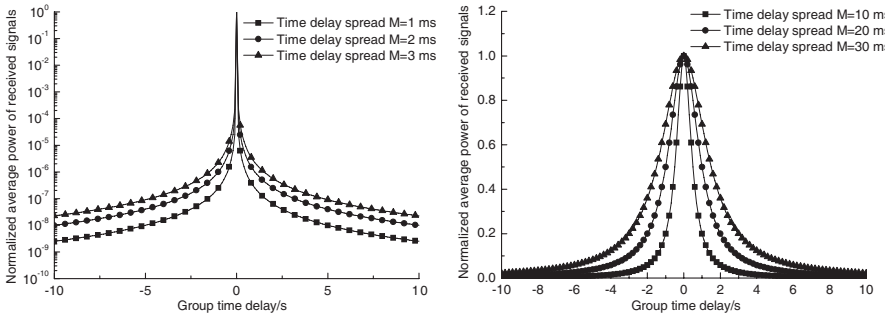

Figure 4. Change in the normalized average power of the received signal $\bar{I}$ with group time delay and multi-path time delay spread M. The normalized average value of time delay power spectrum $\bar{\tau} = 0$ and the transmitting signal power $\alpha = 1\,\mathrm{J/s}$.

When the multi-path time delay spread M is of a certain value (here, $M = 2\,\mathrm{ms}$) for the same group time delay, the larger is the average power of the transmitting signal, the greater is the normalized average value of the received signal power, which is easy to understand (Figure 6).

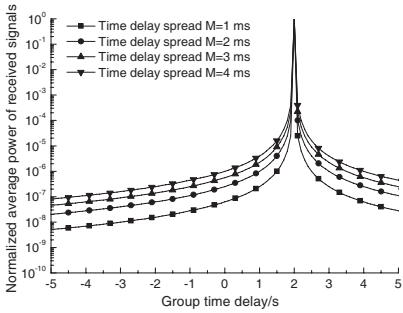

Figure 5. Change in the normalized average power of the received signal $\bar{I}$ with group delay and multi-path time delay spread M. The normalized average value of the time delay power spectrum $\bar{\tau} = 2\,\mathrm{s}$ and the transmitting signal power $\alpha = 1\,\mathrm{J/s}$.

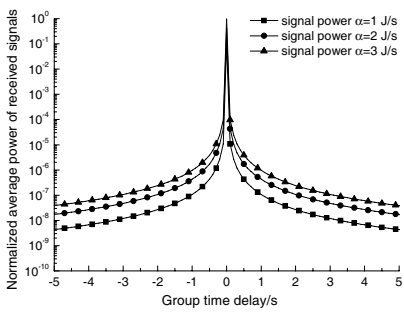

Figure 6. Change in the normalized average power of the received signal $\bar{I}$ with group time delay τ and average transmitting power α. The normalized average value of time delay power spectrum $\bar{\tau} = 0$ and the multi-path time delay spread $M = 2\,\mathrm{ms}$.

3.3. Change in the Variance of the Multi-path Time Delay $\sigma_\tau^2(I)$ with the Normalized Power of the Received Signal

As shown in Figure 7, the larger is the multi-path time delay spread M, the greater is the variance of the multi-path time delay $\sigma_\tau^2(I)$. Meanwhile, with the increase in the normalized power of the received signal, the signal variance rapidly decreases and then slowly decreases. The larger is the multi-path time delay spread, the more dispersive is the time delay power spectrum and the greater is the corresponding multi-path time delay variance. Moreover, the greater is the normalized instantaneous power of the received signal, the stronger is the received signal. Thus, the signals that originate from different paths are very close to the same phase. The time delay spectrum of the signal is narrower, and its signal variance is smaller.

4. EXPERIMENTAL ANALYSIS

The amplitude of the multi-path time delay spread of the ionospheric channel is related to the signal energy distribution of different propagation modes, and to the relative time delay of the multi-mode propagation and its space distribution [31]. Both the signal energy distribution and the relative time delay are closely associated with the ratio K which is the operating frequency of the basic maximum

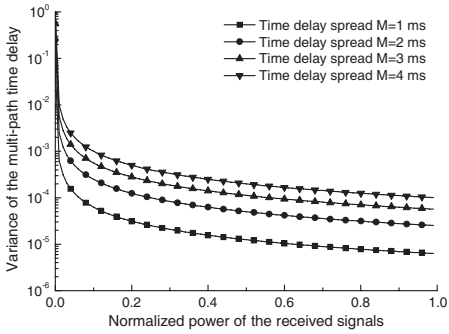

Figure 7. Change in the variance of the multi-path time delay $\sigma_\tau^2(I)$ with the normalized power of the received signals and multi-path time delay spread M.

usable frequency (MUF). In practical engineering application, the time delay spread of the HF ionospheric channel is typically measured by twice of the standard deviation of the projection of the time domain of the channel transfer function, which can be measured by the sweep-frequency pulse sounding technique. Asiyo and Afullo have obtained the multi-path fading occurrence in five cities in South Africa by multi-path measurements over a 6.73 km Line-of-Sight (LOS) link [32]. To further analyze the probability density distribution of the multi-path time delay, three space radio paths with different distances along the east-west direction are analyzed at different times and seasons. The measured value of the time delay spread is obtained by the sweep-frequency pulse sounding technique. The changes in the probability density distribution of the multi-path time delay and its average value with time delay spread and the ratio K are discussed. The main performance parameters for the experimental circuit system are shown in Table 1.

At the beginning of the experiment, the radar signal originated from the transmitting and receiving units is fed to the A/D converter (Figure 8). Then, each pulse is sampled for 16 ms at a sampling rate of 10 ms. At the same time, synchronization is conducted, i.e., sky wave signals are not received during the first 1.6 ms of the 16 ms sampling time. The 16 average sub-sampling signals obtained are used to estimate the noise (i.e., noise sub-sampling). The rest of the sub-samples are signal sub-samples. To ensure that noise signals are not mistaken as the signals under study, threshold, time correlation and frequency correlation tests (Figure 8) are conducted. Then, the sampling signal is input to the computer to calculate the average value

Table 1. Main performance parameters of the experimental circuit system.

Main Performance Parameters	
Frequency Range	15 MHz
Stepped-Frequency Interval	200 kHz
Pulse Width	1 ms
Detection Pulse Number Per Frequency	4
Transmit Power	3 kW
Transmitting Antenna Gain	17 dB
Receiving Antenna Gain	2.8 dB

of the four sampling pulse signals for each frequency. A total of 160 average sub-samples signals Z_i are obtained for each round of sampling. Finally, the multi-path time delay spread can be calculated using the following formulas [33].

$$I = \sum_{i=17}^{160} Z_i \quad \text{signal power} \tag{21}$$

$$\langle I \rangle = \frac{\sum\limits_{i=17}^{160} i \cdot Z_i}{\sum\limits_{i=17}^{160} Z_i} \quad \text{first-order moment} \tag{22}$$

$$\langle I^2 \rangle = \frac{\sum\limits_{i=17}^{160} i^2 \cdot Z_i}{\sum\limits_{i=17}^{160} Z_i} \quad \text{second-order moment} \tag{23}$$

$$M = \sqrt{\langle I^2 \rangle - \langle I \rangle^2}/5 \quad \text{time delay spread} \tag{24}$$

As shown in Equation (24), the time delay spread of the channel is closely related to the first and second moments of the received signal power. For the three measured circuits, more than tens of thousands of measurement data are obtained. After the statistical averaging process of these data using Equations (21) to (24) and different K ratios, the probability density distribution of the multi-path time delay spread can be obtained.

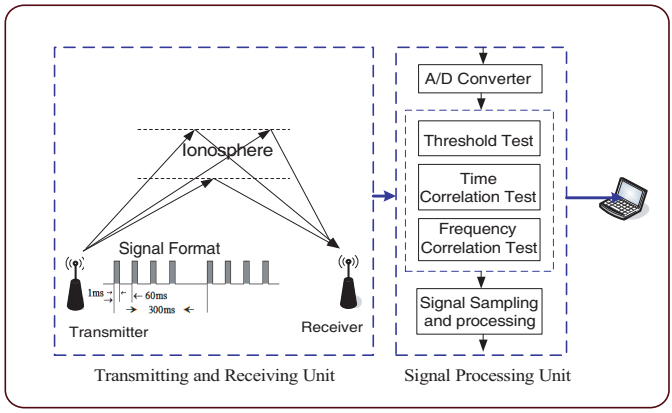

Figure 8. Experimental principle scheme for measuring the multi-path time delay.

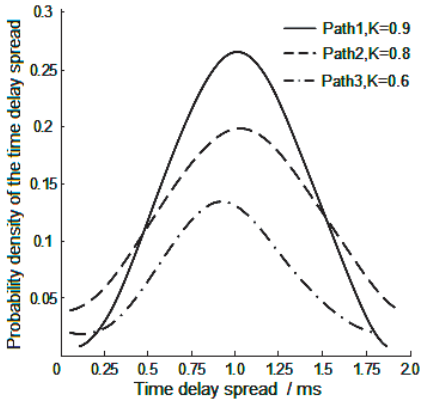

Figure 9. Probability density distribution of the multi-path time delay spread of the three radio paths.

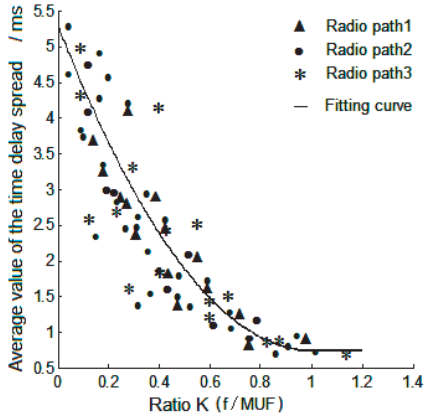

Figure 10. Change in average time delay spread with the ratio K for the three radio paths.

The changes in the probability density distribution of the multi-path time delay spread with different radio paths and different K ratios (here, $K = 0.9$, $K = 0.8$ and $K = 0.6$) are shown in Figure 9. Although the path length and working season for the three test circuits are different, the probability density distribution of the time delay spread for the three radio paths approximately follows a normal distribution,

for a specific ratio K. This result is consistent with that in the literature [33–35].

The changes in the average time delay spread M_{mean} with the ratio K for the three radio paths are shown in Figure 10 (where ▲, •, and $*$ denote the data from the three different radio paths, and the solid line represents the fitting curve obtained by the measured data). The average time delay spread M_{mean} decreases with the increase in ratio K, and reaches a minimum value in the vicinity of the ratio $K = 0.9$. This minimum value is maintained until the operating frequency reaches the MUF of this circuit. Moreover, the minimum value of the average time delay spread for the three radio paths is very close. As shown by the data point distribution, although the path lengths for the three radio paths are different, the difference in the average time delay spread among the different radio paths is less than 0.2 ms when the ratio K is larger than 0.65. With further increase in ratio K, this difference decreases. When ratio $K > 1.0$, this difference does not exceed 0.1 ms. Some studies suggest that when the variation quantity of the time delay spread is greater than 0.5 ms, the error rate of the HF transmission is more obvious because of the increase in the multi-path time delay spread [33]. Using the LS method, the relationship between the average time delay spread M_{mean} and ratio K for different radio paths is fitted as

$$\begin{cases} M_{mean}(K) = \frac{1}{2f}(K - 1.0)^2 + 0.7\,\text{ms} & \text{K} < 1.0 \\ M_{mean}(K) = 0.7\,\text{ms} & \text{K} \geq 1.0 \end{cases} \tag{25}$$

where $M_{mean}(K)$ represents the average time delay spread and f the focal point parameters of the parabolic curve.

Figure 10 shows that the fitting curves of the three different circuits are substantially the same. Thus, in engineering applications with general accuracy, Equation (25) can be used to calculate the multi-path time delay spread for a given operating frequency radio path. The relationship between the average time delay spread $M_{mean}(K)$ (Figure 10) and its standard deviation σ is shown in Figure 11. Considering that the actual operating frequency is generally greater than 0.7-fold of the basic MUF, the observation data greater than 0.7-fold of the MUF are fitted. The result is represented by the solid line in the figure. The changes in the time delay standard deviation with the average time delay spread $M_{mean}(K)$ can be approximately expressed by a line with a slope of 0.36, i.e., $\sigma = 0.36 M_{mean}(K)$. The root mean square deviation between the observed data and Equation (25) is less than 0.08 ms.

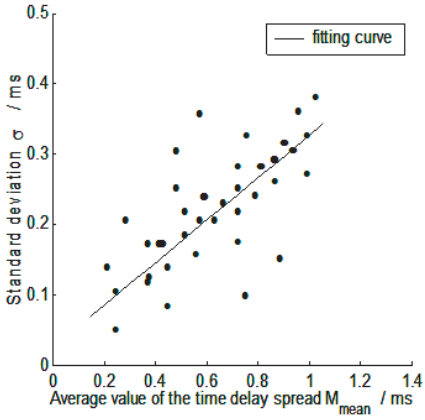

Figure 11. Relationship between the average time delay spread and standard deviation σ.

5. CONCLUSION

The HF ionospheric channel is a multi-path time delay channels whose signal fading follows the Rayleigh distribution. In this study, the probability density distribution of the multi-path time delay, average power of the received signal, and signal variance change with the time delay spread (or Doppler shift spread) are derived using Rayleigh fading, after which they are discussed. The theoretical and experimental research shows that the multi-path time delay spread for a specific frequency approximately meets a normal distribution, and the average time delay spread decreases with the increases in the ratio K for a given radio path. Meanwhile, regardless of the changes in the group delay and multi-path time delay, the probability density of the multi-path time delay can reach a maximum value at the normalized average value of the time delay spectrum $\bar{\tau}$. This finding indicates that the multi-path time delay is most likely the average value of the time delay spectrum. Moreover, the smaller the multi-path time delay spread M is, the faster its signal power decreases. Thus, the smaller the multi-path time delay spread is for a channel, the smaller the jitter range of the received signal power is. The experimental results also prove that the multi-path time delay spread for a specific frequency approximately follows a normal distribution. Theoretical and statistical results indicates that for a given radio path, the proposed procedure may be used to roughly estimate the probability of the signal time delay spread $P(M(K) > M_0)$, which is greater than a given value M_0.

First, the basic MUF for a given time is calculated on the basis of the latitude and longitude of the launch and receiving points [34, 35]. Then, the average time delay spread $M_{mean}(K)$ for a specific frequency is calculated using Equation (25). Finally, the probability density of the time delay spread, which is greater than or equal to a certain value M_0 (i.e., $P(M(K) \geq M_0)$, is obtained based on the feature of the normal distribution. This study provides an empirical method for further predicting and estimating the multi-path time delay for a specific frequency radio path.

6. FUTURE WORK

This study focuses on the statistical relationship between the ionospheric channel parameters, but does not significantly consider the influence of the other parameters of the ionosphere, such as the rapid electron density fluctuation of the ionospheric irregularities, ionospheric drift velocities, and geomagnetic effects. The effect of other ionospheric factors on the multi-path time delay and Doppler shift should be considered. Some studies have initially conducted research on this topic [36–38], and this field is a future research direction for us.

ACKNOWLEDGMENT

This work was supported by the Ocean Public Welfare Scientific Research Project, State Oceanic Administration People's Republic of China (No. 201005017), the Specific Research Project Foundation of the Education Department of Shaanxi province (No. 2012JK1002), and the Xi'an Polytechnic University Project (No. 2012KJ148).

REFERENCES

1. Kandic, M. and G. E. Bridges, "Limits of negative group delay phenomenon in linear causal media," *Progress In Electromagnetics Research*, Vol. 134, 227–246, 2013.
2. Bello, P. A., "Characterization of randomly time-variant linear channels," *IEEE Transactions on Communications Systems,* Vol. 11, No. 4, 360–393, 1963.
3. Maresca, J. W. and T. M. Georges, "Measuring rms wave height and the scalar ocean wave spectrum with HF skywave radar," *J. Geophys. Res.*, Vol. 85, No. 26, 2759–2771, 1980.
4. Bell, B. M. and T. E. Ewart, "Separating multipaths by global optimization of multidimensional matched filter," *IEEE*

Transaction on Acoustics, Speech, and Signal Processing, Vol. 34, No. 5, 1029–1037, 1986.

5. Zhang, W., A. Hoorfar, and L. Li, "Through-the-wall target location with time reversal MUSIC method," *Progress In Electromagnetics Research*, Vol. 106, 75–89, 2010.
6. Zhang, X., G. Feng, and D. Xu, "Blind direction of angle and time delay estimation algorithm for uniform linear array employing multi-invariance MUSIC," *Progress In Electromagnetics Research Letters*, Vol. 13, 11–20, 2010.
7. Lizzi, L., F. Viani, M. Benedetti, P. Rocca, and A. Massa, "The M-DSO-ESPRIT method for maximum likelihood DOA estimation," *Progress In Electromagnetics Research*, Vol. 80, 477–497, 2008.
8. Ching, P. C. and H. C. So, "Two adaptive algorithms for multipath time delay estimation," *IEEE Journal of Oceanic Symposium on Circuits and Systems*, Vol. 19, No. 3, 458–463, 1994.
9. Qi, C., Z. Zhao, W. Yang, Z.-P. Nie, and G. Chen, "Electromagnetic scattering and Doppler analysis of three-dimensional breaking wave crests at low-grazing angles," *Progress In Electromagnetics Research*, Vol. 119, 239–252, 2011.
10. Zhang, G. G., J. Wang, H. W. Li, and H. Huang, "Improved blind source extraction for time delay estimate in passive coherent location system," *Progress In Electromagnetics Research B*, Vol. 37, 257–274, 2012.
11. Shin, D. C. and C. L. Nikias, "Estimation of frequency-delay of arrival (FDOA) using fourth-order statistics in unknown correlated Gaussian noise source," *IEEE Transactions on Signal Processing,* Vol. 42, No. 10, 2771–2780, 1994.
12. Cheng, J., G. Gao, W. Ding, X. Ku, and J. Sun, "An improved scheme for parameter estimation of G° distribution model in high-resolution SAR images," *Progress In Electromagnetics Research*, Vol. 134, 23–46, 2013.
13. Booker, H. G., J. A. Rateliffe, and D. H. Shinn, "Diffraction from an irregular screen with application to ionosphere problem," *Phil. Trans. Roy. Soc.*, Vol. 242, No. 856, 579–607, 1950.
14. Essex, E. A. and F. H. Hibberd, "Auto-correlation of the fading of multiple echoes from the ionosphere," *J. Atmos. Terr. Phys.,* Vol. 29, No. 8, 1025–1027, 1967.
15. Baussard, A., M. Rochdi, and A. Khenchaf, "PO/MEC-based scattering model for complex objects on a sea surface," *Progress In Electromagnetics Research*, Vol. 111, 229–251, 2011.
16. Wang, Y., Y.-M. Zhang, and L.-X. Guo, "Microwave Doppler

spectra of sea echoes at high incidence angles: Influences of large-scale waves," *Progress In Electromagnetics Research B*, Vol. 48, 99–113, 2013.

17. Nie, D., M. Zhang, X. Geng, and P. Zhou, "Investigation on Doppler spectral characteristics of electromagnetic backscattered echoes from dynamic nonlinear surfaces of finite-depth sea," *Progress In Electromagnetics Research*, Vol. 130, 169–186, 2012.
18. From, W. R. and D. H. Meehan, "Mid-latitude spread-F structure," *J. Atmos. Terr. Phys.*, Vol. 50, No. 7, 629–638, 1988.
19. Cornelius, D. W. and E. A. Essex, "HF Doppler observations associated with spread F," *J. Geophys. Res.*, Vol. 84, No. 4, 1361–1368, 1979.
20. Long, X. L. and J. C. Hou, "On the frequency variation of radio waves reflected from the ionosphere," *Acta Geophysica Sinica*, Vol. 22, No. 4, 388–395, 1979 (in Chinese).
21. Ma, L., Z.-F. Li, and G. Liao, "System error analysis and calibration methods for multi-channel SAR," *Progress In Electromagnetics Research*, Vol. 112, 309–327, 2011.
22. Davies, K. and D. M. Baker, "On frequency variations of ionospherically propagated HF radio signals," *Radio Science*, Vol. 1, No. 5, 545–556, 1966.
23. Lee, J.-H., S.-W. Cho, S.-H. Park, and K.-T. Kim, "Performance analysis of radar target recognition using natural frequency: Frequency domain approach," *Progress In Electromagnetics Research*, Vol. 132, 315–345, 2012.
24. Liu, Z.-Y. and L.-X. Guo, "A quasi three-dimensional ray tracing method based on the virtual source tree in urban microcellular environments," *Progress In Electromagnetics Research*, Vol. 118, 397–414, 2011.
25. Bennet, J. A., "The calculation of Doppler shifts due to a changing ionosphere," *J. Atmos. Terr. Phys.*, Vol. 29, No. 887–891, 1967.
26. Papoulis, A., *Probability, Random Variables and Stochastic Processes*, 4th Edition, S. Unnikrishna Pillai, McGraw-Hill Europe, January 2002.
27. Ma, X. Y. and C. L. Nikias, "Joint estimation of time delay and frequency delay in impulsive noise using fractional lower-order statistics," *IEEE Transactions on Signal Processing*, Vol. 44, No. 11, 2669–2686, 1996.
28. Davies, K., *Ionospheric Radio Wave*, Peter Peregrinus Ltd., London, United Kingdom, 1990.
29. Stein, S., "Statistical characterization of fading multipath

channels," Report No. 321, Sylvania Applied Research Lab., Waltham, Massachusetts, 1963.

30. CCIR, "Ionospheric propagation and noise characteristics pertinent to terrestrial radio communication systems design and service planning (Fading)," *Reports of the CCIR*, Vol. VI, No. 266-7, 298–316, 1990.
31. Zhong, X.-M, C. Liao, and W. Lin, "Time-delay-based multi-target detection and power delivering," *Progress In Electromagnetics Research M*, Vol. 19, 25–38, 2011.
32. Asiyo, M. O. and T. J. O. Afullo, "Statistical estimation of fade depth and outage probability due to multipath propagation on southern Africa" *Progress In Electromagnetics Research B,* Vol. 46, 251–274, 2013.
33. Daly, R. F., K. D. Felperin, T. I. Dayharsh, et al., "Curts phase II automatic frequency selection system-signal processing," *Application and Evaluation. Final Report,* AD-815884/2, 1967.
34. CCIR, "Ionospheric sounding at oblique incidence, propagation in ionized media," *Recommendations and Reports of the CCIR*, Vol. VI, Report 249-5, Int. Telecommunication Union, Geneva, 1986.
35. CCIR, "Propagation predication Method for HF Broadcasting, Propagation in ionized Media," *Recommendations and Reports of the CCIR,* Vol. VI, Report 894, Int. Telecommunication Union, Geneva, 1986.
36. Guier, W. H., "Ionospheric contributions to the Doppler shift at VHF from near-earth satellites," *Proc. IRE*, Vol. 49, No. 11, 1680–1681, 1961.
37. Ignatenko, M. V. and M. V. Tinin, "Influence of ionospheric irregularities on the form of radio signal scattering spectrum in over-the-horizon radar sounding of the rough sea surface," *Waves in Random Media,* Vol. 13, No. 3, 151–164, 2003.
38. Willman, J. F., "Frequency-dependent ionospheric refraction effects on the Doppler shift of satellite signals," *IEEE Trans. Aerospace and Electronic Systems*, Vol. 1, No. 3, 283–289, 1965.